ISTITUTO NAZIONALE DI FISICA NUCLEARE
Laboratori Nazionali di Frascati

LNF-83/103

D. Bisello et al. : A MEASUREMENT OF $e^+e^- \to \bar{p}p$ FOR $(1975 \leq \sqrt{s} \leq 2250)$ MeV

Estratto da:
Nuclear Phys. B224, 379 (1983)

Servizio Documentazione
dei Laboratori Nazionali di Frascati
Cas. Postale 13 - Frascati (Roma)

Nuclear Physics B224 (1983) 379–395

A MEASUREMENT OF $e^+e^- \to \bar{p}p$ FOR ($1975 \leqslant \sqrt{s} \leqslant 2250$) MeV

D. BISELLO, S. LIMENTANI, M. NIGRO, L. PESCARA, M. POSOCCO and P. SARTORI

Istituto di Fisica dell'Università, Padova,
Istituto Nazionale di Fisica Nucleare,
Sezione di Padova, Italy

J.E. AUGUSTIN, G. BUSETTO*, G. COSME, F. COUCHOT, B. DUDELZAK, P. ESCHSTRUTH, F. FULDA, B. GRELAUD, G. GROSDIDIER, B. JEAN-MARIE, S. JULLIAN, D. LALANNE, V. LEPELTIER, C. PAULOT, R. RISKALLA, P. ROY, F. RUMPF, L. STANCO and G. SZKLARZ

Laboratoire de l'Accélérateur Linéaire, Orsay, France

R. BALDINI and G. CAPON

Laboratori Nazionali di Frascati dell'INFN, Italy

Received 16 May 1983

The $e^+e^- \to \bar{p}p$ cross section has been measured in the energy interval ($1975 \leqslant 2E \leqslant 2250$) MeV for $|\cos\theta| < 0.7$. The measurement is based on ~ 100 events, thus improving by a factor 3 on the previous existing statistics in this energy interval. The form factor $|G|^2$ is given as a function of energy under the assumption $|G_E| = |G_M|$. We also give the first measurement of the differential cross section, averaged over the energy interval, and estimate the ratio $|G_M|/|G_E|$ from it.

1. Introduction

We have measured the $e^+e^- \to \bar{p}p$ cross section in the energy interval ($1975 \leqslant 2E \leqslant 2250$) MeV for $|\cos\theta| < 0.7$. The measurement was performed at the Orsay DCI intersecting storage rings with the DM2 detector. The differential acceptance was better than 90% up to $|\cos\theta| = 0.6$.

Approximately 500 nb^{-1} nominal luminosity was collected between 1975 and 2250 MeV, in steps of 5 MeV, in two series of runs in March and June 1982. The average luminosity was 30 nb^{-1}/day.

* Now at Istituto di Fisica dell'Università di Padova.

A total of ~ 100 events with essentially no background has been collected, thus improving by a factor ~ 3 on the previously existing statistics in this energy interval with a geometrical acceptance at least 40% higher in $\cos\theta$ and 5 times higher over all.

2. Apparatus

The experiment has been performed at the DCI intersecting storage rings with the DM2 detector. The detector has been extensively described elsewhere [1] and we only recall here its main characteristics. It is schematized in fig. 1. A solenoidal magnet with a field of 5 kG, uniform to better than 1%, 2 m in diameter and 3 m in length, is filled with 2 cylindrical MWPC, 140 and 240 mm in radius respectively, followed by 13 drift chambers with radii increasing from 325 to 871 mm. Five of the drift chambers have wires parallel to the solenoid axis, while the remaining 8 have a pitch of $\pm 3°$. Still inside the field there follows a layer of 36 4 cm water Čerenkov counters, and 36 matching scintillators $20 \times 164 \times 2500$ mm in size, equipped for TOF and $\mathrm{d}E/\mathrm{d}x$ measurements (S-counters).

Outside the solenoid coil there is a photon detector subdivided in 8 sectors (octants), each of which contains 14 layers of streamer tubes [2] for a total of 672 tubes/sector separated in groups of 4 + 4 + 3 + 3 planes by 5 layers of 3 scintillator counters each. A total of 14 layers of lead, the first eight $\frac{1}{4}X_0$ and the following six $\frac{1}{2}X_0$ thick, cause shower development. The magnet coil itself is ~ 0.8 X_0 thick.

The angular acceptance of the drift chambers is $\Delta\phi = 360°$, $25° \leqslant \theta \leqslant 155°$; that of the photon detector is $\Delta\phi = 350°$, $45° \leqslant \theta \leqslant 135°$.

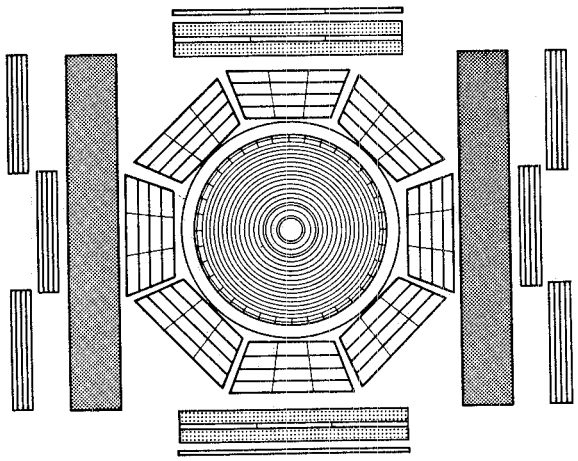

Fig. 1. Schematic front view of DM2.

The drift chamber resolution is $\leqslant 200$ μm. The momentum resolution at the $\mu\mu$ peak is $\Delta p/p = 2\%$.

The muon detector was not operating and the end cap detectors were not used in this experiment.

3. Trigger

At the low end of the energy interval considered, the proton and antiproton stop in the Čerenkov counters and therefore do not reach the scintillator counters. It was not possible therefore to build a fast trigger based on the proton and antiproton themselves.

A loose trigger based partially on the antiproton annihilation products was then built, which required a hit in the first proportional chamber and the coincidence of one of the S-counters with any two photon counters. Table 1 gives the pattern of the hit counters for the $\bar{p}p$ events and shows that the trigger requirements were effectively loose.

Correction for trigger inefficiency due e.g. to all neutral $\bar{p}$ annihilation in the energy range where the proton and antiproton themselves did not hit the S-counters was made by Monte Carlo simulation and found to be smaller than 5%.

4. Event analysis

The data analysis had the twofold aim of identifying the $\bar{p}p$ signal and of providing a suitable normalization. For the latter, it was decided to use the μ pair events that offer the advantage of being quite similar to the $\bar{p}p$ events as far as

TABLE 1
Pattern of hit counters for $\bar{p}p$ events

No. of hit S counters	0	1	2	3	4	5	6	7	8	9	10	11	12	13	14	15
7															1	
6			1					2	1	4		2				
5			1		1	4	2	1	3	5	1	3			1	1
4					1	2	3	4	2		2	1	1	2		
3			1		4	5	3	2	6	1	1	5	1	1	1	2
2						1	4	1	3		4	1		2		1
1					1											
0														1		

No. of hit γ counters

The area left and below the marked lines was excluded by trigger requirements. The single event in it came in through an alternative trigger condition (neutral trigger).

reconstruction efficiency goes and have an acceptance less critical on the geometrical cuts than the Bhabha e^+e^- pairs. Bhabha events were however identified and counted.

In subsect. 4.1 we discuss the rejection of cosmic and accelerator radiation background; in subsect. 4.2 the identification of collinear events, a class to which belong both the $\bar{p}p$ and the $\mu\mu$, ee pairs. Subsect. 4.3 describes the identification of the Bhabha events and therefore the separation of the $\mu\mu$ signal from them. Subsect. 4.4 accounts for the separation of the μ pairs from the residual cosmic background. Finally, subsect. 4.5 discusses the separation of the $\bar{p}p$ events, essentially by the range signature, from a residual low-momentum background.

4.1. ELIMINATION OF COSMIC RAY AND RADIATION NOISE BACKGROUND

Cosmic ray background was first reduced by cutting the time of flight to ± 6 ns between opposed photon counters, magnetic field effects having been taken into account. A further reduction was obtained by an upper cut of 1 cm in the minimum distance between the "collinear tracks" and the beam line. Some additional criteria, that will not be discussed in detail here, allowed rejection e.g. of cosmic ray particles that had emitted a δ ray.

Triggers due to machine noise were partially filtered by requiring some "order" in the chamber signals and were later completely eliminated in the stage of track reconstruction.

A small residual cosmic ray background remained in the data after the above described filters, mostly piled around a particular, low value of momentum. It was eliminated from the $\bar{p}p$ sample by range and subtracted from the $\mu\mu$ sample; the subtraction amounted to $\sim 2\%$.

4.2. IDENTIFICATION OF THE COLLINEAR EVENTS

The procedure for pattern recognition in the proportional and drift chambers is discussed in detail elsewhere [3]. When an event was recognized as two charged tracks, total charge zero and satisfied the following criteria:

(i) the two projected momenta equal within 4 std deviations;

(ii) the two azimuthal angles equal within 4 std deviations;

a fit of both projected tracks in the plane normal to the magnetic field to a common circle was tried.

Cuts to 5% in the χ^2 probability of the fit to the circle and to 0.2 rad in the difference in polar angle between the two tracks (to allow for radiative corrections) were applied to $\mu\mu$ and Bhabha events. The first cut was not applied to $\bar{p}p$ candidates, in view of the fact that the probability was computed taking into account multiple Coulomb scattering appropriated for mesonic tracks, but underestimated for baryonic tracks of the same momentum.

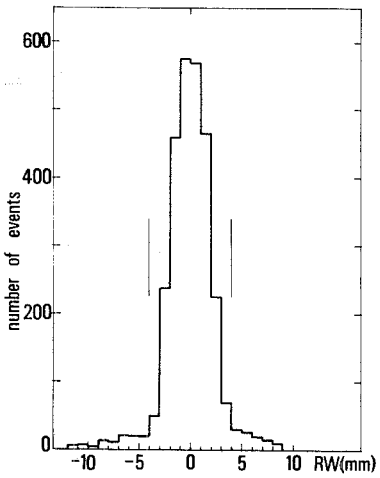

Fig. 2. Radial coordinate of the point of minimum distance between collinear tracks and beam line (RW).

The events were further classified according to whether the vertex was or not inside a fiducial volume chosen on the basis of the colliding beams intersection region and of the measurement errors.

Figs. 2 and 3 give the minimum distance of the common circle from the beam line (RW) and the along-the-beam coordinate (ZW) for the events inside the fiducial volume. The cuts defining the fiducial volume are indicated on the figures. RW has a

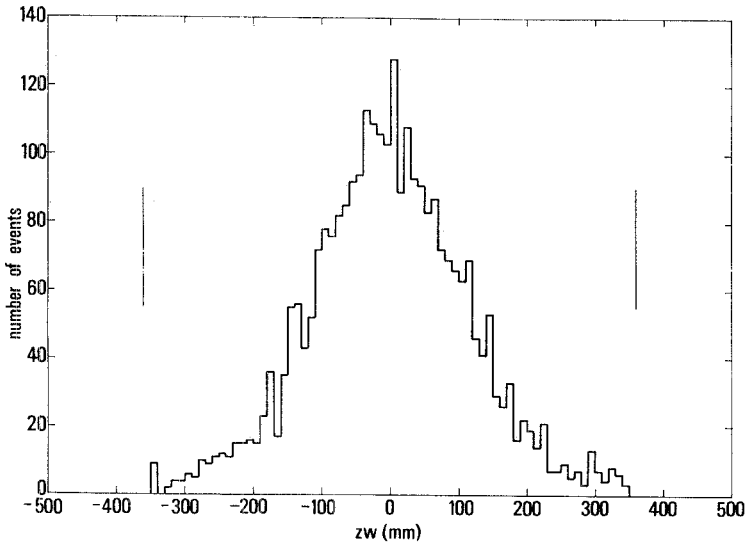

Fig. 3. Along-the-beam coordinate of the same point (ZW).

sign indicating whether the point of minimum distance of the circle from the beam line was on the same or on the opposite side of the centre of curvature.

Inspection of a sample of collinear events outside the fiducial volume showed that they are essentially cosmic rays and they were rejected.

4.3. BHABHA PAIR IDENTIFICATION

Bhabha pairs and $\mu^+\mu^-$ pairs are kinematically indistinguishable. The signature of Bhabha events used in the context of this paper was based on the difference between the number of hit tubes and the number of hit planes in the external photon detector. If we number as "1" the sector of the photon detector that has the maximum value for this variable for a given event, as 2, 3, ... 8 the other sectors in counter-clockwise order and make a plot of the variable versus the octant number so defined, we obtain table 2.

From it one can easily see the collinear character of the events since the next-to-maximum value of the variable corresponds to the octant directly opposed to "1" in the vast majority of the events with some spills in the two adjacent octants.

We denote in the following as ARG1 and ARG2 the difference no. of tubes minus no. of planes summed over the two triplets of octants centered respectively on octant 1 and octant 5.

We then define the potential length in the photon detector as the distance between the exit point from the magnet coil and the exit point from the photon detector of the prolongation in a straight line of the charged track from the median plane of the coil.

Fig. 4 is the scatter plot of $ARG_{1,2}$ and of the corresponding potential length. A step is clearly seen for the potential length of 660 mm that corresponds to normal crossing of the photon detector, indicating that for a smaller potential length the shower does not have full opportunity to develop. We have cut all events with a potential length below 660 mm. Needless to say, the same cut was applied in the Monte Carlo simulation.

Fig. 5 is the scatter plot of ARG1 and ARG2 for events in the Bhabha pairs kinematical region. This is defined by a cut of ± 3 std deviations from the expected momentum value on either track. A clear separation between shower-like and track-like events emerges. We have counted as Bhabha events those for which either ARG1 or ARG2 or both were larger than 10. A very small e^+e^- contamination is left in this way in the remaining events. In the final $\mu\mu$ sample it is less than 2%.

A sample of events for which ARG2 was smaller than 10 (but ARG1 was larger) was visually controlled and proved to be due to electron pairs where one of the electrons fell in the insensitive region between two octants.

4.4. MUON SEPARATION

Fig. 6 gives the mass-squared distribution of the two tracks versus the total energy for all the events left after the cuts described in the previous paragraph: namely,

TABLE 2

Number of hit octant tubes minus number of hit octant planes as a function of octant number for a sample of events; octant "1" corresponds to the maximum value of the variable

⩾ 50	27							
49	14							
48	18							
47	21							
46	24				1			
45	39							
44	42							
43	46				1			
42	80							
41	93				1			
40	119				3			
39	148				10			
38	169				6			
37	238				17			
36	289			1	37	1		
35	326				31	1		
34	326			3	43	1		
33	348			1	64	6		
32	413			7	101	11		
31	444			5	110	7		
30	427			5	109	9		
29	477			11	172	11		
28	484			16	175	12		
27	489			18	238	10		
26	413			18	237	21		
25	417			24	253	22		
24	379			28	265	31		
23	337			28	273	36		
22	316			32	253	46		
21	299			30	251	35		
20	247			37	236	44		
19	214			31	242	36		
18	188			29	236	32		
17	189			34	215	45		
16	128			33	216	38		
15	142			37	202	47		
14	129			32	183	39		
13	116			30	152	37		
12	111			30	137	25		
11	87	1	1	31	127	30		
10	96	1		28	116	37		
9	59		1	33	125	44	1	
8	68	1		34	117	29		
7	34	1		38	107	36		1
6	35	1		35	119	41		4
5	45	2	1	35	122	41	1	5
4	49	3		49	146	57		4
3	96	10	5	65	163	81		8
2	154	21	3	97	268	102	2	29
1	230	139	12	245	540	239	29	128
0	232	642	130	705	1102	692	114	606
	1	2	3	4	5	6	7	8

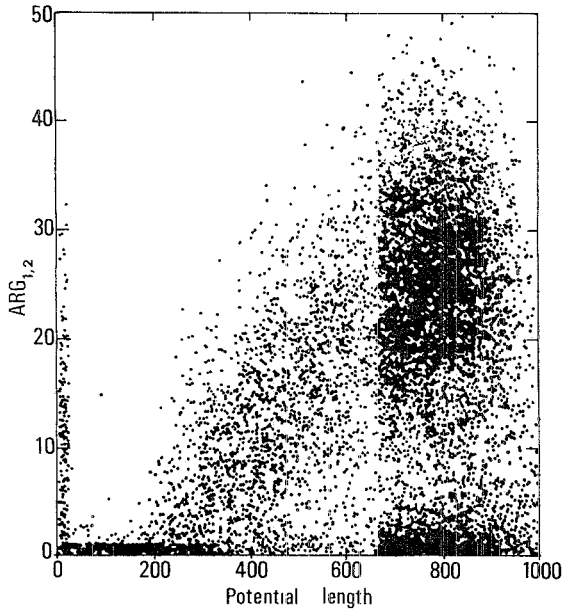

Fig. 4. $ARG_{1,2}$ as a function of the potential octant length. See text definition of ARG.

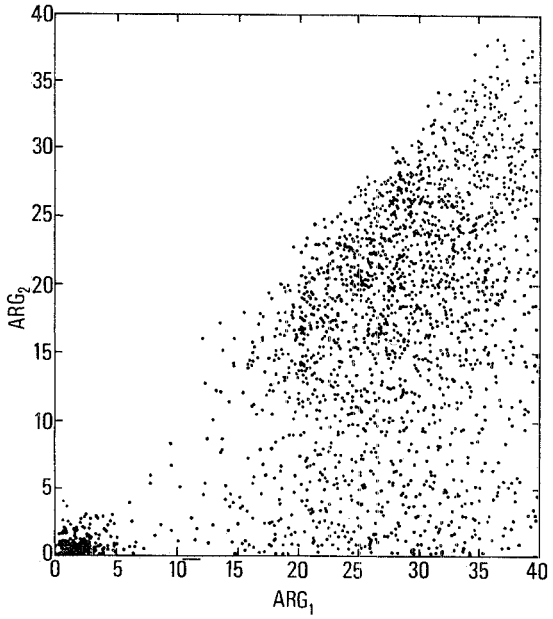

Fig. 5. Scatter plot of ARG1 and ARG2. Figs. 2 to 5 are for samples of events.

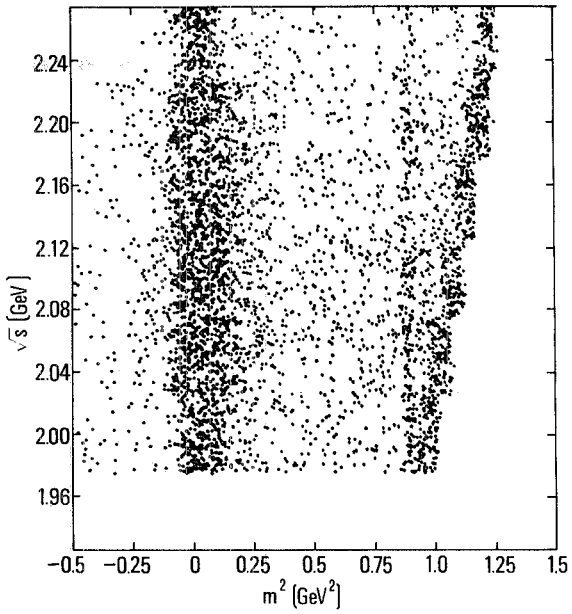

Fig. 6. Squared mass distribution for non-Bhabha, potential-length-cut events, versus $\sqrt{s}$.

collinear events in the fiducial volume with potential lengths in the photon detector larger than 660 mm and no electron signature. The $\mu\mu$ and $\bar{p}p$ lines are clearly seen and so is a low-momentum background that moves with energy in this plot.

The background is reduced by a cut to ± 4 ns in the time of flight to the S-counters and to 4 mm in the distance of the tracks to the beam line. Fig. 7 gives the time of flight distribution for events with $m^2 > 0.6$ GeV^2.

Fig. 8 gives the squared mass distribution after the cuts. One can distinguish the $\mu\mu$ peak, asymmetric and slightly displaced as expected because of radiative corrections.

The proton-antiproton signal emerges from the low-momentum background. A flat small background due to residual cosmic radiation is also still present. In order to minimize the uncertainty in background subtraction due to the radiative μ events present in the high tail of the μ mass spectrum, we have counted as μ events, to be corrected by the acceptance computed by a Monte Carlo simulation with the same cuts, all the squared masses between -0.14 and $+0.02$ GeV^2 from which a background measured by the counts of the bins between -0.30 and -0.14 has been subtracted. The subtraction is $\sim 2\%$.

A residual 2% contamination from e^+e^- events was estimated from the pulse height in the photon detector scintillation counters, and confirmed visually by inspecting a sample of μ events. Monte Carlo simulation indicated the same value. The data have been accordingly corrected.

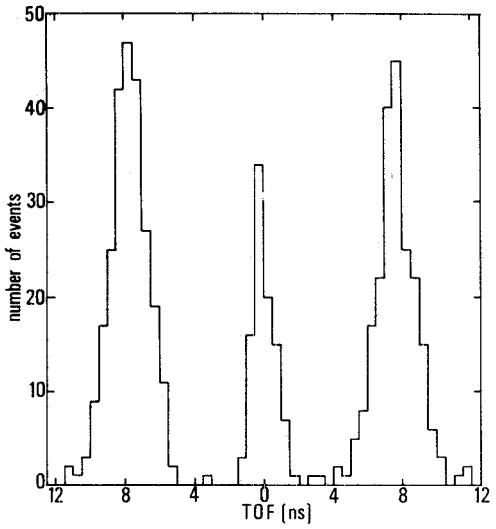

Fig. 7. S-counters time of flight distribution for $m^2 > 0.6$ GeV^2.

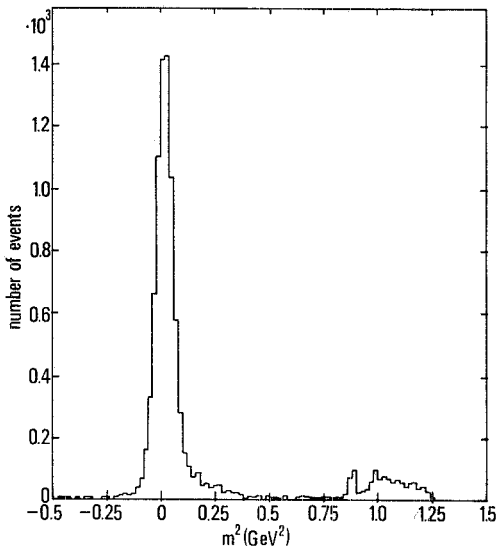

Fig. 8. Squared mass distribution for non-Bhabha events after cuts (see text).

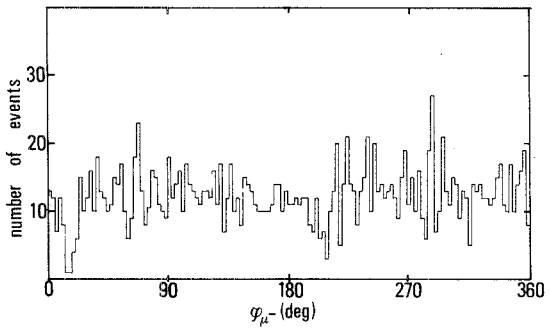

Fig. 9. Azimuthal angle distribution for μ_-.

Fig. 9 gives the azimuthal distribution of the $\mu\mu$ sample. One can see that it is uniform, as expected for true μ pairs with no beam polarization.

4.5. $\bar{p}$p SEPARATION

As mentioned in sect. 2, for a part of our sample, the proton and antiproton came to rest or interacted in flight in the Čerenkov counter or even before. We could therefore not rely on the Čerenkov, or on the time of flight signatures, in order to select the $\bar{p}$p events, although for the higher energies these signatures confirmed the nature of the selected $\bar{p}$p. On the contrary, the range signature is powerful and valid for the whole sample, the highest-energy baryons coming to rest, if they do not interact in flight, in the magnet coil.

The range signature was implemented by requiring that both the positive and the negative track did not continue in the photon detector. "Continuation" was defined in several ways, all leading to the same selection of events.

The range signature foreseeably leads to excluding a small sample of good events for which one annihilation product casually aligns with the parent antiproton. This could be corrected by Monte Carlo simulation, but in view of the small statistics we have preferred a different procedure. Having gained confidence in the visual characteristics of the annihilation from the range-signed events, we have visually inspected all the events with squared mass higher than 0.8 GeV^2 and have so found and added to our sample the $p\bar{p}$ events that had failed the range signature. They amounted to 10% of the total statistics.

Fig. 10 gives the mass squared distribution of all accepted events.

5. Monte Carlo simulation

A Monte Carlo program was used to calculate the total and differential acceptance for the Bhabha, $\mu^+\mu^-$ and $\bar{p}$p events.

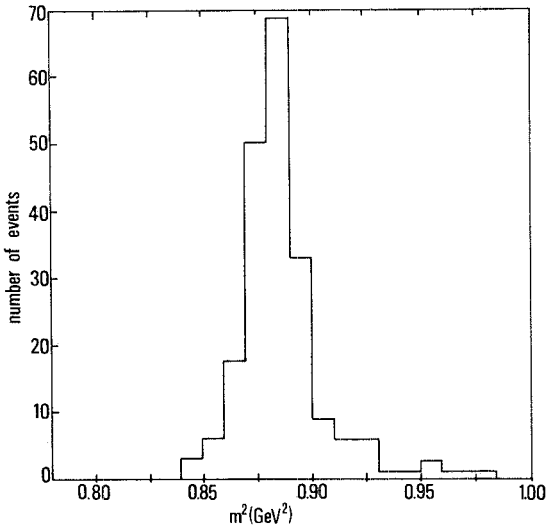

Fig. 10. Squared mass distribution of $\bar{p}p$ sample.

The Bhabha and $\mu^+\mu^-$ events were generated according to the well-known angular distributions, while for the $\bar{p}p$ pairs the distribution corresponding to $|G_E| = |G_M|$ was used. Radiative corrections were applied to all channels.

Particles were then followed through the apparatus simulating restricted energy loss; δ-ray production; multiple Coulomb scattering, complete with correlation between position and angle deviations; bremsstrahlung for the electrons; pair formation for the photons; nuclear interaction for all hadrons and annihilation for the antiproton. These last items, in particular the characteristics of the antiproton annihilation from which the trigger efficiency depends, are discussed in detail below. Hardware cuts were simulated at this level, while the software cuts were applied after the simulation of the measurements errors.

Antiproton momenta in our experiment ranged from ~ 300 to ~ 600 MeV/c. In order to simulate their absorption in the detector material, we have used the measurements of Aihara et al. [4] and the interpolating formula that they found to hold between 0.5 and 280 GeV. The same authors, whose measurements are for $\bar{p}$ of 485 and 597 MeV/c on carbon, aluminum and copper, find that the black disk model for nuclei is valid in this momentum range to reproduce the A dependence of the cross section.

Whenever an antiproton was absorbed in flight or came to rest, it was assumed to annihilate. Final state multiplicity has been studied in detail for annihilation on a free proton at rest and at 1.6 GeV/c [5] and found to have a very slow dependence on energy.

Bugg et al. [6] and Besch et al. [7] have studied experimentally the pion re-absorption effect in the parent nucleus when the annihilation takes place on a bound

nucleon. The effect is found to be modest, ranging from $11 \pm 1\%$ for carbon, to $22 \pm 1.4\%$ for lead and can be reproduced with a smooth A dependence for the π survival probability.

For the surviving pions, a distribution of energy loss due to nuclear effects in the parent nucleus has also been simulated according to the experimental data of ref. [8].

Once outside the parent nucleus, the annihilation pions were tracked through the apparatus and their nuclear interaction probability was simulated according to the measured cross sections of Ashery et al. [9].

The simulation included nuclear cascade effects according to the model of Grant et al. [10]. The products of the nuclear cascades, in particular relatively fast nucleons, and the proton from the $e^+e^- \to \bar{p}p$ reaction were also tracked through the apparatus. The proton cross sections used are from ref. [11].

The $p\bar{p}$ acceptance as a function of $\sqrt{s}$ is reported in table 3. The μ pair acceptance was 0.56 ± 0.02.

6. Experimental results

Fig. 11 gives the angular distribution of the $\mu^+\mu^-$ events. The agreement with the expected $(1 + \cos^2\theta)$ behaviour is quite good and is in itself an indication of the

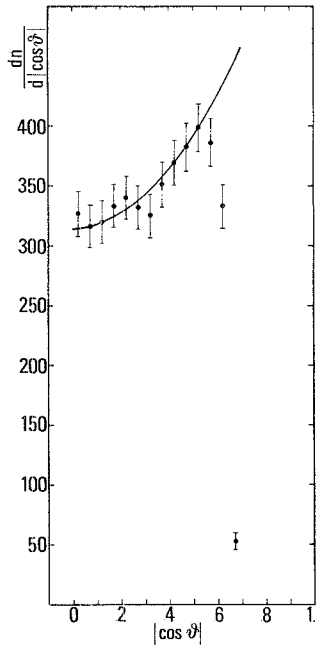

Fig. 11. μ angular distribution. The curve is $\int(1 + \cos^2\theta)\,\mathrm{d}\cos\theta$, normalized to the total number of events with $|\cos\theta| < 0.5$.

sample not being contaminated by cosmic ray and better still by Bhabha background.

The measured $\mu^+\mu^-$/Bhabha ratio within the acceptance cuts has been found to be constant through the experiment and equal to $0.07 \pm 0.001 \pm 0.002$ (the first error being statistical, the second systematic and expressing the uncertainty of background subtraction, and on the cut in probability of the geometrical fit) and must be compared with the Monte Carlo prediction of 0.066 ± 0.002.

We consider the agreement quite satisfactory, especially in view of the skewness of the Bhabha angular distribution.

Table 3 gives for each energy bin the Bhabha, $\mu^+\mu^-$ and $\bar{p}p$ events found, the $\bar{p}p$ acceptance, and the calculated cross section and form factor under the assumption $|G_E| = |G_M|$. We remind the reader that cross sections were computed by normalization to the $\mu\mu$ events. Cross sections are also reported in fig. 12 and form factors in fig. 13 together with the results of previous experiments [11–13].

Fig. 14 gives the differential cross section of the $\bar{p}p$ events, together with some fits to it.

The $|G_E| = |G_M|$ assumption is quite compatible with our data, giving a χ^2 probability of 64%. The best fit gives $|G_M|/|G_E| = 0.34$ with a χ^2 probability of 74%.

In comparing the results of the different experiments, it should be noted that they have all been computed with acceptances derived for isotropic distributions ($|G_E| = |G_M|$). However, no experiment had full $\cos\theta$ coverage. Castellano et al. [13] quote $0.28 \times 4\pi$ for their acceptance, having come down from the $0.6 \times 4\pi$ of their design because of the extended collision region, i.e. because of an effective cut in $\cos\theta$. Delcourt et al. [14] had a useful $|\cos\theta| < 0.5$ coverage. If indeed the angular

TABLE 3

$\sqrt{s}$ (MeV)	$\langle q^2 \rangle$ (GeV^2)	(a) Bhabha	(b) $\mu\mu$	(c) $a \times \Sigma_b/\Sigma_a$	(d) $\int \mathcal{L} dt$	(e) $\bar{p}p$	(f) Acceptance $\bar{p}p$	σ(no.)** for $\lvert G_E\rvert = \lvert G_M\rvert$	$\lvert G\rvert$
1975–2025	4.0	9545	694	680	56.	22	0.52 ± 0.02	0.76 ± 0.16	0.26 ± 0.03
2025–2075	4.2	12216	885	886	77.	24	0.56 ± 0.02	0.56 ± 0.11	0.22 ± 0.02
2075–2125	4.4	12153	861	882	80.	20	0.58 ± 0.02	0.44 ± 0.10	0.19 ± 0.02
2125–2175	4.6	11980	840	869	82.	17	0.58*	0.35 ± 0.09	0.17 ± 0.02
2175–2225	4.8	9903	697	720	71.	19	0.58 ± 0.02	0.45 ± 0.10	0.19 ± 0.02
2225–2250	5.0	2873	205	208	21.	3	0.58*	0.24 ± 0.14	0.14 ± 0.04
		58660	4182						

*Interpolated.

**$\sigma = \dfrac{(e)/(f)}{(c)/0.56}\,\sigma_{\mu\mu}(\sqrt{s})$.

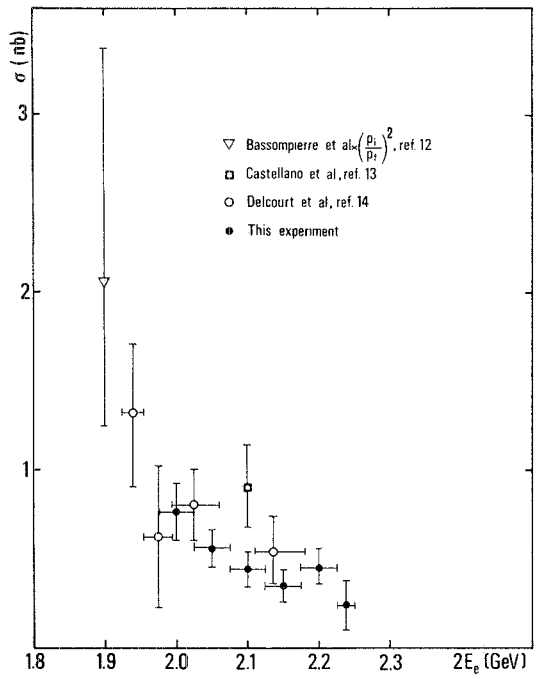

Fig. 12. $e^+e^- \to \bar{p}p$ cross section versus $\sqrt{s}$. Cross sections correspond to acceptance computed from an isotropic distribution. See text for a discussion of this point.

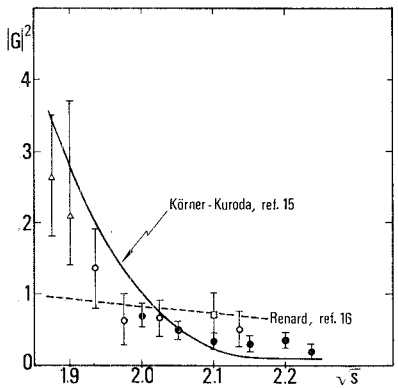

Fig. 13. Form factor versus q^2, under the assumption $|G_E| = |G_M|$.

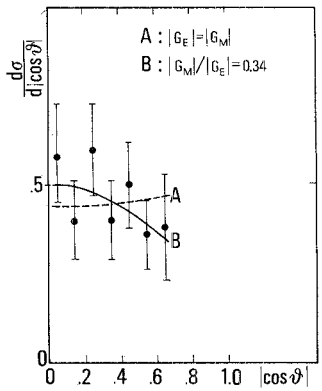

Fig. 14. $\bar{p}p$ differential cross section. $|G_E| = |G_M|$ gives a χ^2 probability of ~ 64%, $|G_M|/|G_E| = 0.34$ (best fit) a probability of 74%.

TABLE 4

$\lvert\cos\theta\rvert$	no. of events	Acceptance	$d\sigma/d\cos\theta$
0–0.1	20	0.94	0.58 ± 0.13
0.1–0.2	14	0.94	0.40 ± 0.11
0.2–0.3	21	0.95	0.60 ± 0.13
0.3–0.4	14	0.96	0.40 ± 0.11
0.4–0.5	17	0.92	0.50 ± 0.12
0.5–0.6	12	0.91	0.36 ± 0.10
0.6–0.7	6	0.43	0.38 ± 0.15
0.7–0.8	1	–	–

distribution should not be isotropic, all total cross sections should be revised and could come to an even better agreement.

In table 4 we give the differential cross section for our whole sample. These results are subject to the assumption $|G_E| = |G_M|$ only in a negligible way.

We thank Professor Perez-y-Jorba, Director of LAL, for his support. We are particularly appreciative of the efforts of the engineers and the technicians of our group. We are indebted to all the LAL technical services for their assistance and especially to the DCI group directed by P. Marin. We thank A. Courau, A. Falvard, B. Michel, J.C. Montret, J. Jousset and Z. Ajaltouni for their help during data taking.

Finally, we thank Dr. A. Grant and O. Botner of CERN for their fast routines of shower development.

References

[1] J.E. Augustin et al., Phys. Scripta 23 (1981) 623
[2] G. Battistoni et al., Nucl. Instr. Meth. 164 (1979) 57;
B. Grelaud et al., Proc. of the 3rd Int. Meeting on proportional and drift chambers (Dubna, 1978) p. 229
[3] G. Capon, Internal notes DM2/R-4/79; DM2/R-21-80; DM2/R-12/81
[4] H. Aihara et al., Nucl. Phys. A 360 (1981) 291
[5] J.E. Enstrom et al., LBL 58, 1972 (compilation);
E. Fett et al., Phys. Lett. 59B (1975) 182
[6] W.M. Bugg et al., Phys. Rev. Lett. 31 (1973) 475
[7] H.J. Besch et al., Z. Phys. A292 (1979) 197
[8] K. Bhabha et al., Nucl. Phys. A 306 (1978) 292
[9] D. Ashery et al., TAUP 836-80
[10] A. Grant, Nucl. Instr. Meth. 131 (1975) 167
[11] P.U. Reubert et al., Nucl. Phys. A 183 (1972) 81
[12] G. Bassompierre et al., Phys. Lett. 68B (1977) 477
[13] M. Castellano et al., Nuovo Cim. 14A (1973) 1
[14] B. Delcourt et al., Phys. Lett. 86B (1979) 395
[15] J.G. Körner and M. Kuroda, Phys. Rev. D60 (1977) 265
[16] F.M. Renard, Phys. Lett. 47B (1973) 361